Cellular in vivo imaging reveals coordinated regulation of pituitary microcirculation and GH cell network function

Chrystel Lafont[a,b,c,d], Michel G. Desarménien[a,b,c,d], Mathieu Cassou[a,b,c,d], François Molino[a,b,c,d], Jérôme Lecoq[e], David Hodson[a,b,c,d], Alain Lacampagne[f], Gérard Mennessier[g], Taoufik El Yandouzi[a,b,c,d], Danielle Carmignac[h], Pierre Fontanaud[a,b,c,d], Helen Christian[i], Nathalie Coutry[a,b,c,d], Marta Fernandez-Fuente[h], Serge Charpak[e], Paul Le Tissier[h], Iain CAF Robinson[h], and Patrice Mollard[a,b,c,d,1]

[a]Department of Endocrinology, Institute of Functional Genomics, Montpellier 34094, France; [b]Centre National de la Recherche Scientifique (CNRS) UMR5203, Montpellier 34094, France; [c]Institut National de la Santé et de la Recherche Médicale (INSERM) U661, Montpellier 34094, France; [d]University of Montpellier, Insitute of Functional Genomics, Montpellier 34094, France; [e]Neurophysiology and New Microscopy Laboratory; Centre National de la Recherche Scientifique (CNRS) UMR8154; Institut National de la Santé et de la Recherche Médicale (INSERM) U603; University of Paris Descartes, Paris 75270, France; [f]Institut National de la Santé et de la Recherche Médicale (INSERM) U637, Montpellier 34295, France; [g]Centre National de la Recherche Scientifique (CNRS) UMR5207, Montpellier 34095, France; [h]Division of Molecular Neuroendocrinology, MRC National Institute for Medical Research, London NW7 1AA, United Kingdom; and [i]Department of Physiology, Anatomy and Genetics, University of Oxford, Oxford OX1 3QX, United Kingdom

Edited* by Tomas G. M. Hökfelt, Karolinska Institutet, Stockholm, Sweden, and approved January 11, 2010 (received for review March 9, 2009)

Growth hormone (GH) exerts its actions via coordinated pulsatile secretion from a GH cell network into the bloodstream. Practically nothing is known about how the network receives its inputs in vivo and releases hormones into pituitary capillaries to shape GH pulses. Here we have developed in vivo approaches to measure local blood flow, oxygen partial pressure, and cell activity at single-cell resolution in mouse pituitary glands in situ. When secretagogue (GHRH) distribution was modeled with fluorescent markers injected into either the bloodstream or the nearby intercapillary space, a restricted distribution gradient evolved within the pituitary parenchyma. Injection of GHRH led to stimulation of both GH cell network activities and GH secretion, which was temporally associated with increases in blood flow rates and oxygen supply by capillaries, as well as oxygen consumption. Moreover, we observed a time-limiting step for hormone output at the perivascular level; macromolecules injected into the extracellular parenchyma moved rapidly to the perivascular space, but were then cleared more slowly in a size-dependent manner into capillary blood. Our findings suggest that GH pulse generation is not simply a GH cell network response, but is shaped by a tissue microenvironment context involving a functional association between the GH cell network activity and fluid microcirculation.

blood flow | hormone pulsatility | oxygen pressure | tissue microenvironment | extracellular space

Pituitary endocrine cells receive blood-borne stimuli and deliver their hormonal outputs via a complex network of capillaries that pervade the gland. The pattern of release of many hormones, such as growth hormone (GH), is an important signal regulating the response of peripheral tissues (1). To achieve a hormone pulse in the circulation, thousands of individual endocrine cells must respond coordinately to regulatory inputs that enter the gland, and the hormones released from individual cells into the extracellular space must then exit the gland as a pulse.

To understand how these hormone pulses are built up in vivo, one must take into account the close link between blood supply, metabolic requirements, and functional activities of pituitary cells (2–5). Oxygen supply by portal vessels is essential for pituitary function (3, 6); however, practically nothing is known about how incoming oxygen is distributed within the gland and whether oxygen intake and consumption are temporally regulated during hormone secretion. The distribution of incoming signaling molecules by the pituitary microcirculation is also a long-standing question: how and to what extent secretagogues can be regionally distributed to their target pituitary cells (4, 5, 7, 8)? Similarly, because there is no experimental description of the fate of hormones between their site of release and final entry into the capillary lumen, studies describing the clearance of released hormones from the gland have so far relied on simulated datasets (9).

Using pituitary slice preparations, we have recently demonstrated the existence of a fully functional GH network in situ (10). However, the mechanisms involved in the shaping of hormone pulses by the GH network in vivo, in a dynamic environment, remain unknown. To date, cellular in vivo imaging of the pituitary has been limited to nonmammalian models (zebrafish) (11), in which the portal blood is absent and the pituitary endocrine cells are directly innervated by hypothalamic neurosecretory cells (12). Live, in vivo imaging of endocrine glands amenable to surgical externalization, such as the islets of Langerhans, has allowed the real-time blood flow in mouse pancreatic islets to be described (13). Similarly, online measurements of partial oxygen pressure with Clark-type oxygen microsensors have already shown that slow changes in $P_{tiss,O2}$ closely correlate with oscillatory insulin secretion both in vivo (14) and in vitro (15, 16). However, none of these technical approaches are easily applicable to deep structures such as the mammalian pituitary gland, which is located on the ventral side of the brain beneath the highly vascularized hard palate. Moreover, in vivo cell identification is needed because the pituitary tissue presents a mosaic of cell types in 2D imaging. Using mice expressing GFP-tagged GH cells (17), we have developed optical imaging methods that can monitor directly in vivo the relationship between the blood vasculature and GH cell network function. These methods involved modifying a fluorescent stereomicroscope with long working distance objectives to image at wide field and single-cell resolution, an exposed pituitary gland deep in its in vivo environment. By combining complex microsurgical approaches in transgenic mice with analytical imaging tools, we show that the GH cell network has a functional association with fluid microcirculation to deliver hormone pulses in living mice.

Author contributions: C.L., J.L., S.C., I.C.A.F.R., and P.M. designed research; C.L., M.G.D., J.L., D.H., A.L., T.E.Y., D.C., H.C., N.C., M.F.-F., and P.L.T. performed research; M.C., F.M., G.M., M.F.-F., and P.L.T. contributed new reagents/analytic tools; C.L., M.G.D., J.L., P.F., and S.C. analyzed data; and D.H., P.L.T., I.C.A.F.R., and P.M. wrote the paper.

The authors declare no conflict of interest.

*This Direct Submission article had a prearranged editor.

Freely available online through the PNAS open access option.

[1]To whom correspondence should be addressed. E-mail: patrice.mollard@igf.cnrs.fr.

This article contains supporting information online at www.pnas.org/cgi/content/full/0902599107/DCSupplemental.

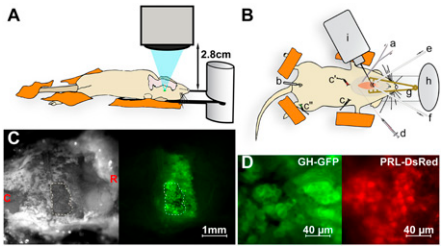

Fig. 1. Cellular in vivo imaging of the pituitary gland in fluorescent protein-tagged transgenic mice with long-range microscopy. (*A* and *B*) Schematics of the experimental arrangement (profile and top views, respectively). (*A*) An air-transmission 20× magnification objective with 2.8 cm working distance is fitted on a fluorescent microscope, equipped with a variable light beam excitation and an EM-CDD camera acquisition setup. It allows real-time in vivo imaging with adaptive final magnification (8-800×) of the ventral side of the pituitary gland surgically exposed in an anesthetized mouse. (*B*) a, Tracheal catheter for motorized ventilation and oxygen and anesthetics supply; b, rectal temperature control; c, heart rate monitor; d, jugular catheter for i.v. injection and blood sampling; e and f, via a small hole in the palate bone, the pituitary surface is continuously irrigated with saline through inlet and outlet tubes, respectively; g, retractor, h, the skull is glued onto a glass slide; i, micropipette holder. (*C Left*) Bright field image of the open palate bone of a GH-eGFP mouse. (*Right*) Corresponding fluorescence image (λex 488 nm). Letters *C* and *R* (in red) indicate the caudal-rostral orientation of the anesthetized animal. The hole in the palatal bone is encircled with a dashed line. (*D*) High-magnification views of the superficial cell layers of pituitaries from anesthetized male GH-eGFP (*Left*) and female PRL-DsRed (*Right*) mice.

Results

Imaging the Pituitary Gland in Vivo with Single-Cell Resolution. The long-range in vivo imaging setup (Fig. 1*A*) provides up to 800× magnification imaging at a 2.8-cm working distance from the lens. To image the pituitaries of anesthetized mice, a ventral surgical approach is made via the palate (*Materials and Methods*). The long working distance beneath the lens allows placement of patch clamp and/or iontophoretic injection pipettes (Fig. 1*B*). Fig. 1*C* shows the exposed ventral pituitary surface of a GH-eGFP transgenic mouse at low magnification under both bright field and epifluorescent illumination. Continuous irrigation of the field with saline avoids tissue heating due to fluorescence excitation light. In real time, the field undergoes large regular excursions due to respiratory movements and systolic pulses. This was countered by developing software that used registration points in the movies to correct these regular whole-field movements (Fig. S1 and Movie S1). Spatial resolution, light excitation, and emission intensities were sufficient to visualize the cellular organization of individual somatotrophs (10) and to distinguish different colored fluorescent reporters for GH (eGFP, secretory vesicles) and Prolactin (DsRed, cytoplasmic) (Fig. 1*D*). Stable images were obtained in vivo for >3 h, and movies at both macro and micro scales were captured in the same experiments using the zoom function on the microscope. In vivo recordings of pituitary regions (*ca.* 200–400 µm diameter), loaded with the fluorescent Ca^{2+} indicator fura-2, showed flickering Ca^{2+} spikes across the entire field (Fig. S2 *A* and *B* and Movie S2), reflecting the spontaneous electrical activity of individual cells (18) maintained under our experimental conditions in vivo ($n = 8$ animals). Cross-correlation analysis of calcium recordings also revealed cell–cell coordination between spontaneously active cells (Fig. S2*C*), as previously reported in acute pituitary slices (19).

Blood Flow Is Spatially Controlled Within the Pituitary. It was also possible to measure both the microvascular architecture and blood flow in the same pituitary field. By i.v. injections of intravascular markers such as 70-kDa dextran labeled with a different color fluorophore (e.g., rhodamine dextrans in GH-GFP mice; Fig. 2*A* and Movie S3) (20), fine vessel structures could be distinguished from the surrounding cells and red blood cells (RBCs), seen as moving nonfluorescent "shadows" within the fluorescent plasma. Software was developed (Fig. S3) to estimate flow rate by measuring RBC velocity in both rectilinear and curvilinear structures, and to compare flow and direction for each capillary imaged. (We recognize that plasma flow may differ from RBC flow, but this distinction is beyond the scope of this study.) Vessel diameters were distributed as a single population (Fig. 2*B*), although a few large vessels were also present (~25 µm diameter; Fig. S4*A*). In contrast to vessel diameters, two populations of RBC velocities were apparent (peaks at 100–200 µm/s and 500–600 µm/s, respectively, $n = 6$ animals, 112 vessels analyzed; Fig. 2*B*). Movies from different regions of the gland revealed a 15-fold variation in flow rates, with a striking 7-fold range in flow rate between vessels of equivalent diameters in different parts of the gland (Fig. 2*C*). It was also evident that capillary branching, tortuosity, and flow vary widely within a gland (Fig. S4). Larger-scale images of intrapituitary vasculature were obtained using rhodamine-gelatin perfusion followed by confocal/two-photon microscopy and 3D reconstruction of fixed GH-GFP glands (10), showing the close proximity of single capillaries and structural GH cell network motifs ($n = 5$ glands; Fig. S5). Using 3D morphometric analysis of fixed gelatin rhodamine-filled GH-eGFP pituitaries (10), we were able to quantify the density of the pituitary gland vasculature (6.5 ± 1.0%, $n = 12$). These large-scale images from deeper regions of fixed pituitary glands were entirely consistent with the local appearance from direct imaging of accessible superficial portions of the living gland in vivo.

We then questioned whether we could measure intrapituitary oxygen tension and how this relates to supply from the rich vasculature in vivo. Measurements of oxygen partial pressure ($P_{tiss,O2}$) were made with Clark-type oxygen microsensors (2- to 5-µm tip diameter) (14, 16, 21–23), which were directly inserted into GH cell clusters in anesthetized GH-eGFP mice ventilated with variable air/O_2 mixtures. Resting $P_{tiss,O2}$ values were 33.8 ± 1.7 mmHg in the presence of atmospheric air ($n = 4$), and increased up to 57.3 ± 5.5 mmHg in a mixture of 50% atmospheric air/50% O_2 ($n = 15$; Fig. S6). When $P_{tiss,O2}$ levels were measured in different regions of the same gland, the differences

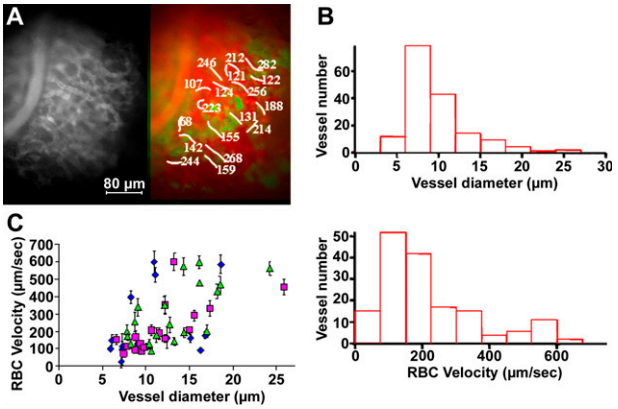

Fig. 2. RBC velocities in the microcirculation of GH-eGFP mice. (*A*) In vivo imaging of rhodamine dextran-labeled vasculature (*Left*) and corresponding RBC velocities in vessel branches (colored in red) in a GH-eGFP (green) pituitary (Movie S3). (*B*) Plots of vessel numbers as a function of vessel diameters (*Upper*) and RBC velocities (*Lower*), respectively. (*C*) RBC velocities as a function of vessel diameters in rostral (green triangles), central (violet circles) and caudal (blue squares) regions of a lateral part of a GH-GFP pituitary. Data are reported as means ± SD.

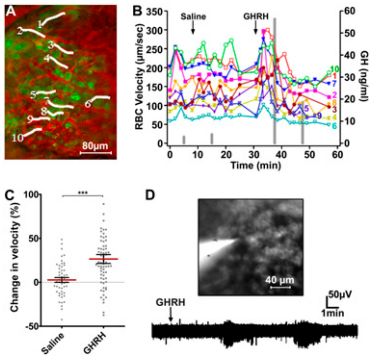

Fig. 3. In vivo GHRH-induced changes in blood flow correlated with GH cell function. (*A*) In vivo imaging of blood flow in a GH-eGFP mouse pituitary. White lines represent vessel branches in which RBC velocities were measured (*B*). (*B*) RBC velocities (left axis) and plasma GH (right axis, vertical gray bars) were sequentially measured before, during, after i.v. injections of saline and GHRH, respectively. (*C*) Distributions of change in velocity (percentage of control RBC velocity) within 5-min periods following i.v. injections of either saline or GHRH. Also represented are means ± SEM for saline and GHRH conditions, respectively (***$P < 0.001$, $n = 8$ animals). (*D Upper*) Extracellular electrical recording of GH-eGFP cells. The patch pipette was filled with a saline solution and Lucifer yellow. (*Lower*) Jugular injection of GHRH (1 μg) triggered recurrent bursts of spikes.

in partial oxygen pressure throughout the regions examined varied from 1 to 6 mmHg ($n = 27$ measurements, $n = 6$ animals).

Changes in Local Blood Flow and Oxygen Partial Pressure Coincide with the Activation of GH Pulses. To test whether secretory activity is coincident with changes in flow rates in capillaries surrounding GH cells, blood flow was monitored before, during, and after an i.v. bolus of GHRH, a specific GH secretagogue ($n = 9$ animals). Fig. 3 *A* and *B* illustrates the results from an experiment imaging the lateral region of a GH-GFP pituitary gland, recording RBC flows in 10 vessels overlying a patch of GH cells, and measuring peripheral plasma GH concentrations, before, during, and after injections of saline or GHRH (Fig. 3*B*, gray bars). GHRH injection increased overall flow rates with some variability in patterns, without alterations in heart rate, around the time of secretion as inferred from the timing of the GH pulse in the peripheral circulation (Fig. 3*B*). To quantify blood flow changes in vivo, the relative changes in RBC flows were compared during a 5-min period after i.v. injection of either saline or GHRH, and showed a significant coordinated increase in RBC flow shortly after GHRH invaded the parenchyma (Fig. 3*C*; $P < 0.001$). It was also possible to obtain extracellular voltage recordings from identified GH cells by inserting a patch clamp electrode into a GH cluster beneath the objective (Fig. 3*D*; $n = 7$ animals). These GH cells showed spontaneous action potentials, and i.v. injections of GHRH (1 μg) triggered repetitive high-frequency bursts of firing ($n = 5$ animals).

Because blood flow controls O_2 supply in the extracellular space (ECS) within GH cell clusters, we monitored $P_{tiss,O2}$ levels before and after i.v. GHRH injection (Fig. 4 *A–G*; $n = 7$ animals). GHRH triggered an increase in $P_{tiss,O2}$ variance ($P < 0.001$, $n = 9$ GHRH injections; Fig. 4*B*, middle traces), without detectable changes in heart rate during acquisition of pituitary $P_{tiss,O2}$ and blood flow measurements (Fig. 4*B*). Strikingly, both upward and downward $P_{tiss,O2}$ deflections (Fig. 4*C*) increased in amplitude (Fig. 4 *D* and *F*) and duration (Fig. 4 *E* and *G*) following GHRH injection, suggesting that both O_2 supply from pituitary capillaries and O_2 consumption by stimulated GH cells were enhanced during GHRH-induced GH secretion. Because blood flow (Fig. S3) was resolved with individual RBC velocity measurements every ~15–30 s, whereas $P_{tiss,O2}$ levels were

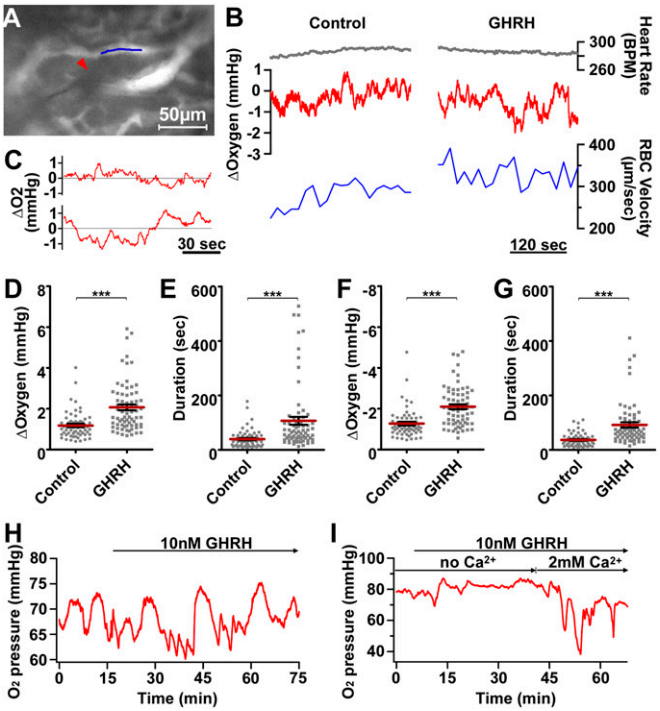

Fig. 4. In situ $P_{tiss,O2}$ responses to GHRH. (*A–G*) In vivo measurements of pituitary $P_{tiss,O2}$ levels with oxygen microsensors in anesthetized GH-eGFP mice. (*A*) The tip (5 μm) of an oxygen sensor (red arrowhead) was inserted into a GH cell cluster (not illustrated). RBC velocity was monitored in a nearby capillary filled (indicated with a blue line segment) i.v. with rhodamine 70-kDa dextran. (*B*) In the same experiment, heart rate (top traces), relative changes in $P_{tiss,O2}$ levels (middle traces), and RBC velocity (bottom traces) were monitored before (*Left*) and after i.v. (*Right*) GHRH injection. (*C*) In another experiment, expanded time-lapse recordings of relative changes in $P_{tiss,O2}$ levels before (top trace) and after (bottom trace) i.v. GHRH injection. (*D* and *E*) Distributions of both amplitude (*D*) and duration (*E*) of upward $P_{tiss,O2}$ deflections measured before (control) and after (GHRH) secretagogue injection. (*F* and *G*) Distributions of both amplitude (*F*) and duration (*G*) of downward $P_{tiss,O2}$ deflections measured before (control) and after (GHRH) secretagogue injection. Represented are the means ± SEM for control and GHRH-stimulated conditions (***$P < 0.001$, $n = 7$ animals). (*H* and *I*) Monitoring of pituitary $P_{tiss,O2}$ levels with oxygen microsensors in acute GH-eGFP pituitary slices perfused with saline solution. (*H*) Large spontaneous downward $P_{tiss,O2}$ deflections occurred within a GH cell cluster. Subsequent bath application of GHRH at 10 nM (top horizontal arrow) induced larger and longer $P_{tiss,O2}$ deflections with superimposed smaller $P_{tiss,O2}$ deflections. (*I*) No large downward O_2 changes occurred in a pituitary slice preincubated with a calcium-free saline solution (with 5 mM EGTA). Ten nanomolar GHRH triggered large downward O_2 changes only when the calcium concentration was restored to 2 mM in the bathing medium.

detected every 0.1 s, we were unable to correlate blood flow with fast changes in $P_{tiss,O2}$ levels.

To uncouple O_2 consumption and supply due to blood flow, we performed similar measurements of $P_{tiss,O2}$ in acute pituitary slices where the GH cell network functionally responds to GHRH application (10), but in the presence of constant O_2 levels in the perfusate (24). In 200-μm GH-eGFP pituitary slices, GH cell network motifs spontaneously displayed much larger and longer downward O_2 deflections than those observed in living mice ($P < 0.001$, $n = 7$ slices). These downward deflections in $P_{tiss,O2}$ were amplified in response to 10 nM GHRH, with long-lasting O_2 deflections being evident ($P < 0.001$; Fig. 4*H*; $n = 7$ slices). These were markedly reduced in the absence of calcium in the bathing medium (with 5 mM EGTA, $n = 4$; Fig. 4*I*).

Taken together, the findings suggest that arrival of GHRH generates intense recurrent bursting activity in GH cells to elicit

a global GH secretory response, and that this is associated with a brief coordinated period of increased local blood flow and a change in partial oxygen pressure within stimulated GH cell network motifs.

Blood Vessel Microcircuitry: A Gatekeeper That Shapes the Distribution of Incoming Signaling Molecules and the Clearance of Secreted Products. To simulate the arrival and distribution of a "pulse" of incoming secretagogue from the portal vein, an i.v. pulse of a fluorescent marker was given during vascular imaging. After i.v. injection of 4 kDa rhodamine-labeled dextran (the size of some hypothalamic peptide secretagogues), rostral large vessels were filled first. Seconds later, many secondary smaller and more tortuous vessels were filled sequentially toward the caudal region of the gland (Fig. S7 and Movie S4; $n = 5$ animals). More surprising was an unexpected graded distribution of dye between neighboring small vessels and parenchymal tissue when fluorescence emission was monitored at higher resolution (Fig. 5*A* and Movie S5; $n = 5$ animals). For these experiments, a fluorescein-labeled 500-kDa dextran was injected subsequently to delineate the capillary microarchitecture and show blood flow rates in individual capillary branches in the same imaged fields (Fig. S8). Shortly after i.v. injection of 4 kDa dextran, the larger vessels were filled sequentially, with no increase in fluorescence in the surrounding parenchyma (Fig. 5*Aa*). A few seconds later, the signal intensity decreased in these vessels, and a distal branch became filled from an out-of-field source. Next, some smaller, more tortuous capillaries became fluorescent, and signal began to appear in intercapillary parenchyma (Fig. 5*Ab*). By 26 s after injection, the majority of small capillaries were filled with the fluorescent marker and parenchymal tissue fluorescence was maximal (Fig. 5*Ac*). We further investigated how the fluorescent 4-kDa marker was distributed within the parenchyma by locally injecting the dye within the ECS in the vicinity of 1–2 vessels. To do so, the 4-kDa marker was iontophoretically applied from the tip of a micropipette into GH-eGFP cell clusters (Fig. 5*B a–d* and Movie S6). Both blood vessel location and flow direction are represented in Fig. 5*Ba*. Following focal delivery, the marker spread only locally within the ECS, entered the capillaries, and was cleared efficiently from the field. The 4-kDa marker spread at an average rate of 10.87 ± 3.90 μm/s to a maximum extent of 82 ± 15 μm from the injection site ($n = 12$). These data provide direct in vivo information on how far and quickly molecules the size of portally delivered hypophysiotropic peptides penetrate the pituitary extracellular space to reach their cellular targets.

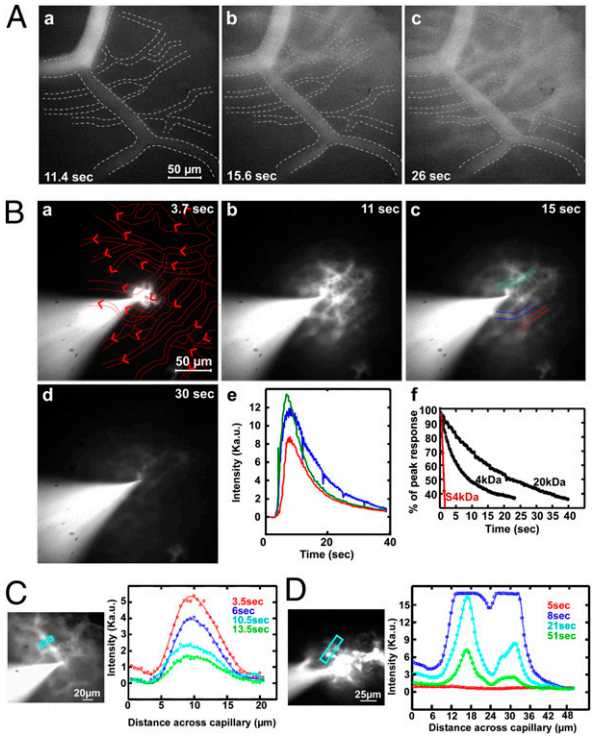

Fig. 5. In vivo imaging of incoming molecules through the microvasculature, fate of products released into the extracellular space, and product clearance at the vascular level. (*A*) Time-lapse imaging of 4-kDa rhodamine dextran in pituitary vessels at high magnification (Movie S5). Values indicate the time delay after i.v. dye injection. Right-left direction shows the rostrocaudal orientation of the gland. Note that fluorescence signal in the parenchyma was detectable only after small vessels became fluorescent (*b* and *c*). See Fig. S8 for associated RBC velocity measurements. (*Ba–d*) Focal release of products was mimicked by iontophoretic injection of 4 kDa rhodamine-labeled dextran (Movie S6). In *a*, maps of microcirculation and blood flow directions (arrowheads) are marked in red. Values indicate the time delay after dye injection. (*e*) Fluorescence intensity as a function of time in three vessels close to the site of dye injection (see vessel locations in *c*). (*f*) Decay times for fluorescence clearance in blood vessels following iontophoretic injections of 4-kDa and 20-kDa fluorescent dyes, respectively. The red line represents a simulation of the 4-kDa dye clearance from the vessel as its measured blood flow. (*C* and *D*) Fluorescence intensity profiles across vessels and nearby perivascular spaces (*Left*, blue windows) after iontophoretic injections of 4-kDa (*C*) or 20-kDa (*D*) rhodamine-labeled dextrans, respectively (see Movie S7 for the 20-kDa injection).

The exit of secreted pulses of hormone from the gland was similarly modeled following iontophoretic injections of fluorescent dextrans, while monitoring uptake, clearance, and flow in nearby vessels as above. Fluorescence signals could be measured within several capillaries across the same field, and showed similar patterns with a single exponential decay time of 8.2 ± 0.3 s following focal delivery of 4 kDa dextran (Fig. 5*Be*; $n = 10$). Similar experiments were performed with 20-kDa dextrans, corresponding to the sizes of pituitary protein hormones such as GH (Fig. 5*Bf* and Fig. 5*D*, $n = 7$ animals). As expected, these larger markers were cleared more slowly, but we noted that even the smallest (4 kDa) was cleared slower than would be expected from its theoretical decay time (*ca.* 0.2–0.5 s) derived by simulation of internal fluorescence clearance from a vessel at its measured blood flow (Fig. 5*Bf*). Furthermore, with injections of larger markers, residual fluorescent dextran appeared to remain in a perivascular region close to the capillary wall during clearance. This could be illustrated by plotting the intensity profiles for 4-kDa and 20-kDa dextrans across the capillary walls delineated in the same images (Fig. 5 *C* and *D* and Movie S7).

Discussion

By imaging the dynamics of locally injected and blood-borne fluorescent markers in GH-eGFP transgenic mice, we describe here a direct functional association between pituitary GH cells and blood vessels in vivo. Using this approach, we have been able to show that the generation of GH pulses by the GH cell network may be influenced by (*i*) the fine regulation of hypothalamic inputs by the pituitary microcirculation; (*ii*) the supply and consumption of oxygen by the vasculature and GH cells; and (*iii*) the dynamic uptake of secreted products by the efferent blood capillaries.

Restricted Pituitary Distribution of Incoming Signaling Molecules. To generate coordinated pulses, secretagogues and inhibitors from the hypothalamus must enter the parenchyma rapidly to reach their targets. Earlier studies have reported that portal blood vessels irrigate distinct pituitary regions (5, 25) and that hypothalamic inputs are not equally distributed within the pituitary microcirculation (4, 7, 8). Here, we modeled this at cellular resolution by (*i*) monitoring the entry rate and distribution of 4-kDa fluorescent markers (mimicking the size of most hypothalamic secretagogues) from the afferent vasculature and (*ii*)

measuring the rate and extent of 4-kDa marker redistribution in the ECS by locally injecting the fluorescent marker between nearby capillaries. Using this 4-kDa marker, there was considerable heterogeneity in the filling rates of capillaries in the same fields, and once the fluorescent marker permeated the parenchyma locally, it spread radially at ~10 μm/s. The extent of diffusion of the 4-kDa fluorescent marker was limited in distance to <100 μm from the injection site, a process which was largely dependent on the rapid penetration into fenestrated capillaries and subsequent clearance into the bloodstream. If the same is true for an endogenous secretagogue, groups of pituitary cells would be exposed to very different secretagogue concentrations when neighboring capillaries emanate from distinct portal vessels (4, 7, 8). This suggests a role for the network organization of GH cells (10) to coordinate cellular response despite heterogeneity in the timing of cell stimulation.

Pituitary Control of Blood Flow and Oxygen Supply: A Component of GH Pulse Generation. Our cellular imaging and sensor studies revealed that the rich capillary meshwork maintains a partial oxygen pressure of ~34 mmHg within the ECS of GH cell clusters. Pituitary oxygen tension was similar to that measured in vivo in mouse pancreatic islets (39 mmHg) (14). We were not able to directly correlate changes in flow rates with partial O_2 concentrations within the gland. For this, further developments, such as laser-guided line scanning, in combination with cellular in vivo imaging, with long-range objectives would be needed to get much higher sampling rates of RBC velocities.

A GHRH bolus triggered recurrent bursting patterns of electrical spikes in GH cells, which were associated with the generation of GH pulses in vivo. Similar, but inversely related bursts of downward deflections in $P_{tiss,O2}$ levels occurred in acute pituitary slices stimulated with GHRH, dependent on extracellular calcium. Both GHRH-induced bursts of $P_{tiss,O2}$ deflections (present study) and coordinated calcium spiking activity (10) recurred with a similar frequency (~20 min). We feel it reasonable to infer that these downward deflections in $P_{tiss,O2}$ levels reflected episodes of O_2 consumption closely associated with calcium-spiking activity of GH cells (10, 17, 18). In vivo, GHRH-induced episodes of O_2 consumption are likely compensated by ongoing increases in O_2 supplies from neighboring capillaries, because downward $P_{tiss,O2}$ deflections were much smaller and mixed with upward $P_{tiss,O2}$ deflections. Together, these findings suggest that the GHRH response in vivo involves recurrent episodes of GH cell activity in the 3D cell network (10), which are associated with periods of O_2 consumption by stimulated GH cell network motifs and O_2 supply from neighboring capillaries.

In this context, the GH cell network shares characteristic features with pancreatic β-cells, which are functionally organized in Langerhans islets (26). The latter display large episodes of O_2 consumption, which are closely associated with β-cell calcium-spiking activities in vitro (21, 22), though they generate smaller and more complex O_2 deflections in vivo (14). In both conditions, slowly evolving O_2 deflections occurred at frequencies similar to those observed for insulin secretion oscillations, supporting a primary role for metabolic oscillations in pulsatile hormone secretion (14–16).

The fact that GHRH-dependent increases in pituitary blood flow rates were temporally coordinated between numerous capillaries in close proximity with GH cell clusters suggests that GHRH can locally regulate blood flow rates. Previous studies have described that GHRH receptors are restrictively expressed in GH cells (27–29), although we cannot exclude the possibility that low levels of receptor may be present in some other pituitary cell types. If GHRH receptors are completely restricted to GH cells, then local alterations in flow are most likely a *consequence* of secretory activity from stimulated GH cells. The effectors of vascular flow change may be pericytes, which display long contractile cytoplasmic processes embracing the endothelial tube of portal capillary vessels (30). These express receptors for diffusible vascular signaling factors (31), such as nitric oxide (32), which is synthesized by GH cells (33, 34).

Perivascular Space: A Time-Limiting Step for Hormone Output. For a coordinated pulse to enter the circulation, secretory bursts must also exit the gland parenchyma promptly. We modeled this in vivo by following clearance of fluorescent markers from the parenchyma into the vessels. Though the passage of markers of similar sizes to pituitary hormones (4 kDa ~ ACTH; 20 kDa ~ GH, PRL) toward blood vessels was rapid, significant amounts of larger markers collected in what appeared to be a perivascular compartment, en route to rapid clearance. This trailing clearance could contribute to the observation that the trailing edges of GH and PRL pulses in vivo tend to be broader than the leading edges, although active inhibition of GH and PRL by somatostatin and dopaminergic systems would also be important to cut off the entry into the parenchyma. Although the pituitary perivascular space (or perisinusoidal compartment) was identified by electron microscopy more than half a century ago (35), its role has been largely neglected, and could even have a local signaling function. For instance, GH released upon acute GHRH stimulation may reside long enough in the perivascular space to control and help maintain the density of blood vessels (36) in close proximity with the GH cell network.

In summary, cellular in vivo imaging of the association of the microcirculation with the GH cell network has highlighted the importance of the vascular microarchitecture and flow to the timing and delivery of input stimuli and oxygen, and the output of a hormonal pulse. The structure and flow dynamics of the pituitary microvasculature will clearly have a large impact on shaping the hormone pulse evoked by the stimulus-secretion coupling events inherent to the long-range endocrine networks that exist in the gland. The cellular in vivo imaging approaches describe here will allow future investigation of how the pituitary microenvironment influences different cell systems, not only during periods of normal physiological demand (e.g., the preovulatory LH surge) but also when the endocrine tissue and microvasculature are altered (e.g., tumors).

Materials and Methods

A brief outline is provided; for full details, see *SI Materials and Methods*.

Animals. Male, 2- to 3-month-old wild-type C57Bl6 or transgenic GH-eGFP mice (17) on a C57Bl6 background were anesthetized by inhalation of isoflurane (1.5% in O_2) or using i.v. injection of ketamine/xylazine (0.1/0.02 mg/g). After dividing the mandibular symphysis, the mucosa overlying the hard palate was parted by blunt dissection under a stereomicroscope to expose an area of palatal periosteal bone. This was thinned with a felt polisher (drill; World Precision Instruments) and then removed with a hook and forceps. The exposed surface of the pituitary gland, visible through the hole in the bone, was continuously superfused with a physiological solution. A jugular venous catheter was inserted for removal of blood samples for RIA of mouse GH and for administration of GH-releasing hormone (GHRH) or fluorescently labeled dextrans. For some studies, female transgenic Prl-DsRed mice were used, which have DsRedExpress protein expression driven by 3.2 kb 5′ and 1.7 kb 3′ of the rat prolactin gene, resulting in lactotroph-specific expression of red fluorescent protein. For hormone assays, 50 μL of blood was sampled before and after 5 and 15 min of an injection of human GHRH 1–29NH_2 (1 μg in vehicle buffer: NaCl 0.9%, heparin 20 unit/mL, and BSA 0.05%) via a jugular vein catheter. Mouse GH was assayed by RIA using mouse reagents kindly provided by the National Institute of Diabetes and Digestive and Kidney Diseases (Bethesda, MD) as previously described (37).

Long Working Distance Imaging with Cellular Resolution and Analysis. Cellular in vivo imaging was performed using a fluorescent stereomicroscope [M2Bio (Carl Zeiss & Kramer Scientific) or StereoDiscovery (Carl Zeiss)] equipped with long working distance objectives. Cytosolic calcium was monitored (38) in cells loaded with the fluorescent calcium dye fura-2/AM after bolus injection via a

micropipette. Electrical activity (39) was monitored with extracellular microelectrodes.

Blood Flow and Oxygen Tension Measurements and Dye Injections. To measure velocities of RBCs in individual capillaries, injections were made via the jugular vein catheter of solutions of dextrans of different molecular weights (from 4.4 to 500 kDa) linked to different colored fluorescent probes: Cascade Blue, FITC, rhodamine, and Texas Red (Molecular Probes and Sigma-Aldrich). To measure partial oxygen pressure ($P_{tiss,O2}$), recordings were made with Clark-type polarographic oxygen microsensors (Unisense) polarized at −0.8 V, as previously reported (23). Fluorescent dextrans were introduced by iontophoresis from a glass micropipette.

Multiphoton and Confocal Imaging of GH-EGFP Pituitaries. Terminally anesthetized mice were perfused via the heart with 3 mL of PBS at 37 °C followed by 6 mL of solution of rhodamine-gelatin (6%) in PBS at a velocity of 1.5 mL/min (40), and pituitaries were prepared for multiphoton and confocal imaging.

ACKNOWLEDGMENTS. The authors thank Elodie Gavois, Alain Carrette, and Philippe Didier for their invaluable assistance. This work was supported by grants from the Institut National de la Santé et de la Recherche Médicale, Centre National de la Recherche Scientifique, the Universities of Montpellier 1 and 2, National Biophotonics and Imaging Platform (Ireland), Réseau National des Génopoles, and Institut Fédératif de Recherches No. 3, Région Languedoc Roussillon, and by core funding from the Medical Research Council (United Kingdom).

1. Waxman DJ, O'Connor C (2006) Growth hormone regulation of sex-dependent liver gene expression. *Mol Endocrinol* 20:2613–2629.
2. Page RB (1982) Pituitary blood flow. *Am J Physiol* 243:E427–E442.
3. Hopkins CR, Farquhar MG (1973) Hormone secretion by cells dissociated from rat anterior pituitaries. *J Cell Biol* 59:276–303.
4. Porter JC, Sissom JF, Arita J, Reymond MJ (1983) Hypothalamic-hypophysial vasculature and its relationship to secretory cells of the hypothalamus and pituitary gland. *Vitam Horm* 40:145–174.
5. Adams JH, Daniel PM, Prichard MM (1965) Observations on the portal circulation of the pituitary gland. *Neuroendocrinology* 1:193–213.
6. Nessi AC, Bozzini CE (1982) Ultrastructural changes in somatotropic cells induced by anemic or hypoxic hypoxia. *Acta Physiol Lat Am* 32:175–183.
7. Nagy GM, Boockfor FR, Frawley LS (1991) The suckling stimulus increases the responsiveness of mammotropes located exclusively within the central region of the adenohypophysis. *Endocrinology* 128:761–764.
8. Nagy GM, DeMaria JE, Freeman ME (1998) Changes in the local metabolism of dopamine in the anterior and neural lobes but not in the intermediate lobe of the pituitary gland during nursing. *Brain Res* 790:315–317.
9. Veldhuis JD, Keenan DM, Pincus SM (2008) Motivations and methods for analyzing pulsatile hormone secretion. *Endocr Rev* 29:823–864.
10. Bonnefont X, et al. (2005) Revealing the large-scale network organization of growth hormone-secreting cells. *Proc Natl Acad Sci USA* 102:16880–16885.
11. Liu NA, et al. (2008) In vivo time-lapse imaging delineates the zebrafish pituitary proopiomelanocortin lineage boundary regulated by FGF3 signal. *Dev Biol* 319:192–200.
12. Pogoda HM, Hammerschmidt M (2007) Molecular genetics of pituitary development in zebrafish. *Semin Cell Dev Biol* 18:543–558.
13. Nyman LR, et al. (2008) Real-time, multidimensional in vivo imaging used to investigate blood flow in mouse pancreatic islets. *J Clin Invest* 118:3790–3797.
14. Bergsten P, Westerlund J, Liss P, Carlsson PO (2002) Primary in vivo oscillations of metabolism in the pancreas. *Diabetes* 51:699–703.
15. Longo EA, et al. (1991) Oscillations in cytosolic free Ca2+, oxygen consumption, and insulin secretion in glucose-stimulated rat pancreatic islets. *J Biol Chem* 266: 9314–9319.
16. Ortsäter H, Liss P, Lund PE, Akerman KE, Bergsten P (2000) Oscillations in oxygen tension and insulin release of individual pancreatic ob/ob mouse islets. *Diabetologia* 43:1313–1318.
17. Magoulas C, et al. (2000) A secreted fluorescent reporter targeted to pituitary growth hormone cells in transgenic mice. *Endocrinology* 141:4681–4689.
18. Schlegel W, et al. (1987) Oscillations of cytosolic Ca2+ in pituitary cells due to action potentials. *Nature* 329:719–721.
19. Guérineau NC, Bonnefont X, Stoeckel L, Mollard P (1998) Synchronized spontaneous Ca2+ transients in acute anterior pituitary slices. *J Biol Chem* 273:10389–10395.
20. Chaigneau E, Oheim M, Audinat E, Charpak S (2003) Two-photon imaging of capillary blood flow in olfactory bulb glomeruli. *Proc Natl Acad Sci USA* 100:13081–13086.
21. Jung SK, Aspinwall CA, Kennedy RT (1999) Detection of multiple patterns of oscillatory oxygen consumption in single mouse islets of Langerhans. *Biochem Biophys Res Commun* 259:331–335.
22. Jung SK, Kauri LM, Qian WJ, Kennedy RT (2000) Correlated oscillations in glucose consumption, oxygen consumption, and intracellular free Ca(2+) in single islets of Langerhans. *J Biol Chem* 275:6642–6650.
23. Lecoq J, et al. (2009) Odor-evoked oxygen consumption by action potential and synaptic transmission in the olfactory bulb. *J Neurosci* 29:1424–1433.
24. Hall CN, Attwell D (2008) Assessing the physiological concentration and targets of nitric oxide in brain tissue. *J Physiol* 586:3597–3615.
25. Porter JC, Hines MF, Smith KR, Repass RL, Smith AJ (1967) Quantitative evaluation of local blood flow of the adenohypophysis in rats. *Endocrinology* 80:583–598.
26. Konstantinova I, et al. (2007) EphA-Ephrin-A-mediated beta cell communication regulates insulin secretion from pancreatic islets. *Cell* 129:359–370.
27. Carmignac DF, Flavell DM, Robinson IC (1996) Pituitary growth hormone-releasing factor receptor expression in normal and dwarf rats. *Neuroendocrinology* 64: 177–185.
28. Morel G, et al. (1999) Restricted presence of the growth hormone-releasing hormone receptor to somatotropes in rat and human pituitaries. *Neuroendocrinology* 70: 128–136.
29. McElvaine AT, Korytko AI, Kilen SM, Cuttler L, Mayo KE (2007) Pituitary-specific expression and Pit-1 regulation of the rat growth hormone-releasing hormone receptor gene. *Mol Endocrinol* 21:1969–1983.
30. Satoh H, Inokuchi T, Shimizu M, Obayashi H, Nakashima Y (1989) Ultrastructure of the hypophyseal portal vessel in mature rats—SEM and TEM observations. *Kurume Med J* 36:91–94.
31. Peppiatt CM, Howarth C, Mobbs P, Attwell D (2006) Bidirectional control of CNS capillary diameter by pericytes. *Nature* 443:700–704.
32. Yemisci M, et al. (2009) Pericyte contraction induced by oxidative-nitrative stress impairs capillary reflow despite successful opening of an occluded cerebral artery. *Nat Med* 15:1031–1037.
33. Kostic TS, Andric SA, Stojilkovic SS (2001) Spontaneous and receptor-controlled soluble guanylyl cyclase activity in anterior pituitary cells. *Mol Endocrinol* 15: 1010–1022.
34. Tsumori M, Murakami Y, Koshimura K, Kato Y (2002) Growth hormone-releasing hormone and gonadotropin-releasing hormone stimulate nitric oxide production in 17beta-estradiol-primed rat anterior pituitary cells. *Endocrine* 17:215–218.
35. Rinehart JF, Farquhar MG (1955) The fine vascular organization of the anterior pituitary gland; an electron microscopic study with histochemical correlations. *Anat Rec* 121:207–239.
36. Sonntag WE, et al. (2000) The effects of growth hormone and IGF-1 deficiency on cerebrovascular and brain ageing. *J Anat* 197:575–585.
37. Carmignac DF, Robinson IC (1990) Growth hormone (GH) secretion in the dwarf rat: Release, clearance and responsiveness to GH-releasing factor and somatostatin. *J Endocrinol* 127:69–75.
38. Stosiek C, Garaschuk O, Holthoff K, Konnerth A (2003) In vivo two-photon calcium imaging of neuronal networks. *Proc Natl Acad Sci USA* 100:7319–7324.
39. Baccam N, et al. (2007) Dual-level afferent control of growth hormone-releasing hormone (GHRH) neurons in GHRH-green fluorescent protein transgenic mice. *J Neurosci* 27:1631–1641.
40. Hashimoto H, Ishikawa H, Kusakabe M (1999) Preparation of whole mounts and thick sections for confocal microscopy. *Methods Enzymol* 307:84–107.